# Modified Monthly Oceanic Rain-Rate Algorithm to Account for TRMM Boost

Long S. Chiu, *Senior Member, IEEE*, Roongroj Chokngamwong, and Thomas T. Wilheit, *Life Fellow, IEEE*

***Abstract*—We provide a modified algorithm for computing Tropical Rainfall Measuring Mission (TRMM) monthly oceanic rain rates (3A11) for TRMM Microwave Imager data using the Microwave Emission Brightness Temperature Histogram (METH) technique developed by Wilheit *et al.* Shin and Chiu examined changes associated with TRMM boost by adjusting the microwave brightness temperature ($T_b$) for the postboost data to match the preboost data. We computed a new relation between $T_b$ and rain rate ($T_b - R$) for the postboost characteristics using the same radiative transfer model of Wilheit *et al.* and modified the algorithm by providing two $T_b - R$ relations for the preboost and postboost era, respectively. The modified algorithm is applied to TRMM data without $T_b$ adjustment. Preliminary results show a significant improvement over the unmodified algorithm in terms of biases and linear trends. Their differences on the application of the METH technique to other microwave data for climate-scale rainfall are discussed.**

***Index Terms*—Global Precipitation Climatology Project (GPCP), microwave radiometry, ocean, rainfall, Tropical Rainfall Measuring Mission (TRMM).**

## I. Introduction

LONG-TERM records of geophysical parameters derived from satellite data have been commonly used in climate studies. These studies include climate trends and variabilities. Climate trends are defined relative to the time period of the data record. If these climate trends are determined using data from different sensors onboard different satellites within the data record, consistency of data sets across sensors and satellites must be guaranteed.

Accurate rainfall and evaporation estimates are crucial to understanding the global water and energy cycles. Over the oceans, satellite estimates are deemed the only means for globally monitoring precipitation due to the scarcity of the buoy data networks. Climate trends are dependent on the time period of record and are sensitive to the input satellite data and algorithms used [4]–[9]. These algorithms should be robust to accommodate changes in the input data to provide a consistent set of outputs for climate-scale trend analysis.

Wilheit *et al.* [1] developed a Microwave Emission Brightness Temperature Histogram (METH) technique for estimating monthly oceanic rain rates based on the Special Sensor Microwave Imager (SSM/I) measurements taken on board the Defense Meteorological Satellite Program (DMSP) satellites. The novelty of the technique is that the rain rates are calibrated to the nonraining portion of the rain spectrum, which is therefore robust to the input satellite data, to the first order. The technique was modified and applied to the Tropical Rainfall Measuring Mission (TRMM) Microwave Imager (TMI) data to create a standard monthly oceanic rainfall product (TRMM reference 3A11).

After the launch in November 1997, the TRMM satellite was boosted from an altitude of 350 km to a higher altitude of 402 km in August 2001 to reduce drag and save maneuvering fuel, thus extending the mission life to at least 2012. The boost has affected the capability of instruments as well as the algorithms and rainfall estimates. For example, the TRMM precipitation radar (PR) echoes near the surface are lower by about 1.2 dB due to the increased distance between the satellite and the surface. Consequently, the ability to detect weak rain by PR is reduced. Tagawa *et al.* [10] have recently provided the method for improved correction of beam mismatch of the TRMM PR after the boost. For TMI, the Earth's incidence angle and the atmospheric path are different between the preboost and postboost period. The brightness temperatures ($T_b$) in the TMI microwave channels have been affected due to the increase in the Earth incidence angle, the footprint diameter, and the swath width. As a result of the slightly longer path between the satellite and the surface, the postboost $T_b$ is relatively higher than the preboost $T_b$. Analyses of Version 6 (current version) TRMM 3A11 rainfall estimates [2] show a distinct jump between preboost and postboost period with respect to the continuous rainfall estimates derived from SSM/I data. Shin and Chiu [2] also provided an ad-hoc adjustment of the microwave $T_b$ for the postboost data by subtracting the increased $T_b$ of 1.67 K for correction of rainfall estimates.

However, in this paper, we provide a modified 3A11 algorithm that takes account of the TRMM boost while no ad-hoc $T_b$ adjustments were made. In essence, the preboost and postboost

Manuscript received October 19, 2009; revised January 19, 2010. Date of publication April 19, 2010; date of current version July 21, 2010. This work was supported by the NASA Tropical Rainfall Measuring Mission Program. The work of R. Chokngamwong was supported in part by the Chinese University of Hong Kong under Direct Grant 2020925 and in part by the Hong Kong Research Grant Council under Grant 447807.

L. S. Chiu is with the Institute of Space and Earth Information Science, Chinese University of Hong Kong, Shatin, Hong Kong, and also with the Department of Geography and Geoinformation Science, College of Science, George Mason University, Fairfax, VA 22030 USA (e-mail: lchiu@gmu.edu).

R. Chokngamwong is with the Institute of Space and Earth Information Science, Chinese University of Hong Kong, Shatin, Hong Kong, and also with the Center for Earth Observing and Space Research, George Mason University, Fairfax, VA 22030 USA (e-mail: roongrojc@yahoo.com).

T. T. Wilheit is with the Department of Atmospheric Science, Texas A&M University, College Station, TX 77843-3150 USA (e-mail: wilheit@tamu.edu).

Color version of one or more figures in this paper are available online at http://ieeexplore.ieee.org.

Digital Object Identifier 10.1109/TGRS.2010.2045505

TMI represent two slightly different sensors and hence, may provide a test of the robustness of the METH approach. To provide a consistent background for comparison, the oceanic rainfall rates estimated by METH using SSM/I data onboard the DMSP F13 satellite are used. The modification of the METH algorithm is explained in Section II, and the results are discussed in Section III. Section IV presents analyses of the rainfall trends computed from the modified 3A11 algorithm and their comparison with SSM/I data. The conclusions are given in Section V.

## II. Modification of METH Algorithm

Details of the algorithm are described by Wilheit *et al.* [1] and Shin and Chiu [2]. The technique relies on brightness temperature–rain rate $(T_b - R)$ relations derived from a radiative transfer model (RTM) [3]. In the RTM, a Marshall–Palmer distribution [11] of raindrops as a function of rain rate is assumed to exist from the ocean surface to the freezing level in the atmosphere. A constant lapse rate of 6.5 °C/km and a relative humidity that increases linearly with height from 80% at the ocean surface to 100% at the freezing level and above are assumed. The variations of sea-surface temperature and emissivity due to surface wind are neglected. A linear combination of twice of the SSM/I vertically polarized brightness temperature at 19.35 GHz minus that at 22.235 GHz is used to reduce the impact of variability of water vapor. At low freezing levels, this linear combination minimizes the dependence of the brightness temperature on water vapor at low rain rates. In the algorithm, the observed microwave $T_b$ histogram is fitted to a mixed lognormal rain-rate distribution. A Gaussian distribution of $T_b$ is assumed for the nonraining part of the $T_b$ distribution, which is described by $T_0$ and $\sigma_0$ (the mean and standard deviation of $T_b$ for the nonraining portion of the $T_b$ histogram). The raining part of the distribution is described by the rain fraction $(p)$, and the mean and standard deviation of the conditional rain-rate distribution. The fitting of the $T_b$ histogram is based on three moments of the distributions (mean, variance, and skewness). The solution is achieved by iteration. At each iteration, all parameters ($T_0$, $\sigma_0$, $p$, and the mean and standard variation of the conditional rain rates) are modified to minimize the errors between the moments. $T_0$ is also used to adjust the difference between the observed and computed $T_b$ histograms. From the relationship, $T_b$ increases with rain rates in the lower rain rates in the emission regime, but decreases for higher rain rates due to scattering of the hydrometeors. Sensor biases between satellites can contribute to biases in rainfall estimates. Since $T_b$ increases with rain rate for the frequently observed rain-rate range, a low bias in $T_b$ would result in a lower rain rate, and vice versa. The solution for $T_0$, to a first approximation, cancels the effect of these biases on the rain rate but not on the freezing level.

The freezing level is considered as a proxy of the columnar humidity content. The METH algorithm uses the mean of the upper 99th percentile of the combined channels of vertically polarized brightness temperatures to determine the altitude of the freezing level. To correct the "beam-filling error," a freezing-level-dependent beam-filling correction (BFC) factor based on modeling and empirical results of Wang [12] and Chiu *et al.* [13] is used. Even though corrections of microwave $T_b$ play a major role to rain-rate increases, Shin and Chiu [2] demonstrate that corrections of the BFC factor can contribute to an increase of about 1.5% of 3A11 rain rates. Therefore, the increase in the BFC due to changes in resolution, as discussed in Shin and Chiu [2], is incorporated in the modified algorithm.

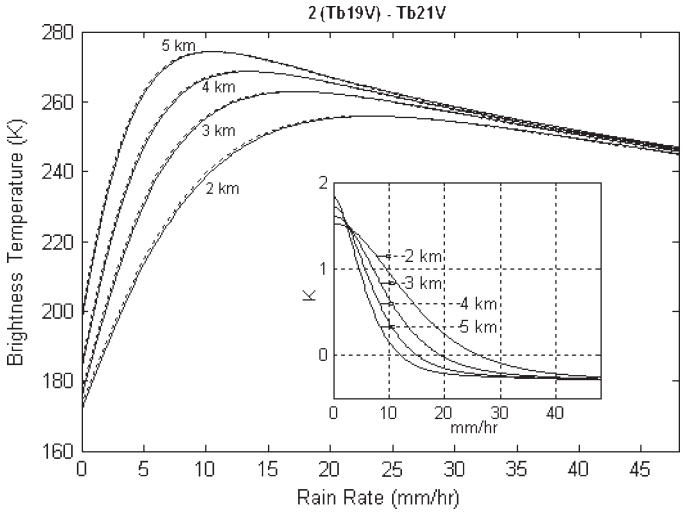


Fig. 1. Relation between brightness temperature (twice vertical polarization at 19.35 minus 21.3 GHz) and rain rate at different freezing levels. The solid and dotted lines represent the relations for the preboost and postboost periods, respectively. The inset shows the difference in the $T_b - R$ relation in brightness temperatures between postboost and preboost orbital configurations.

Using the Wilheit *et al.* [3] model, the $T_b - R$ relations for TRMM preboost and postboost periods are calculated for different freezing levels. Fig. 1 shows the relations of the linear $T_b$ combination (twice that of vertical polarization of 19.35 GHz minus 21.3 GHz of TMI channels) with rain rates for four different freezing levels. The Earth incidence angles are 52.8° and 53.4° for the preboost and postboost periods, respectively. The $T_b$ increases with increasing rain rate and reaches a maximum faster for the higher freezing levels.

The postboost and preboost $T_b - R$ curves are similar, with $T_b$ differences of from $-0.5$ to 2 K for the entire rain-rate domain (see inset in Fig. 1). The computed $T_b$ [and the $T_b$ difference] for postboost is higher than that for preboost at lower rain rates and decreases as rain rate increases. Similarly, the observed $T_b$ at all TRMM microwave frequencies is also higher for postboost period due to the increase of the satellite altitude and the Earth incidence angle [2]. Instead of adjusting the microwave $T_b$ for the postboost data to match the preboost data, we herein provide two $T_b - R$ relations separately for the preboost and postboost periods in the 3A11 oceanic rainfall algorithms.

## III. Results

The rain rates computed using the METH algorithm from SSM/I data of DMSP F13 satellite, which serve as an input to produce the Global Precipitation Climatology Project (GPCP) multisatellite rainfall product [14], are used as a baseline to

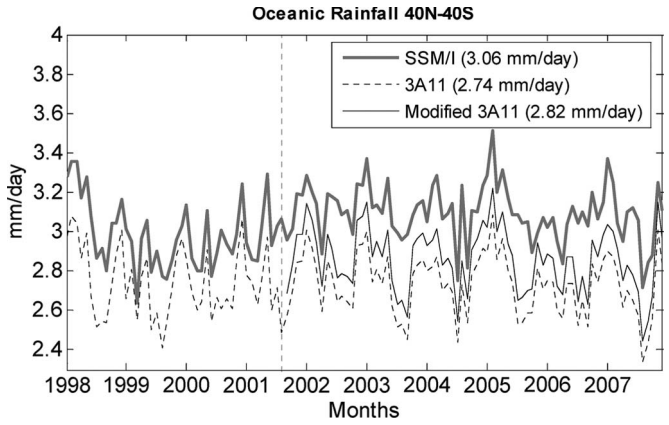


Fig. 2. Time series of rain rates from SSM/I, 3A11, and modified 3A11 from 1998 to 2007. The numbers shown in the box are the mean rain rate for the whole period. The mean rain rates for only the postboost period are 3.10, 2.73, and 2.86 mm/day for SSM/I, 3A11, and modified 3A11, respectively.

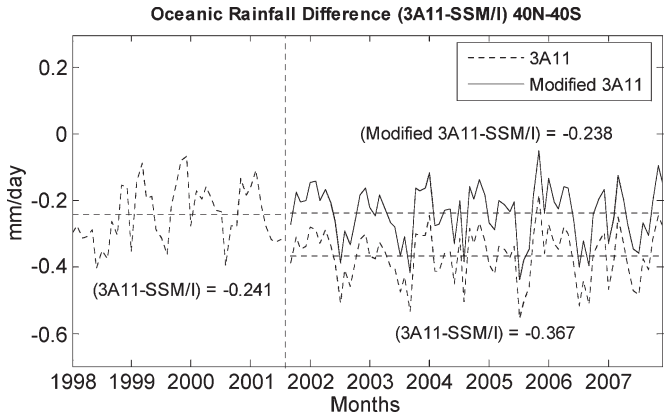


Fig. 3. Differences with SSM/I rain rates of 3A11 and modified 3A11. The mean differences for preboost and postboost periods are computed without August 2001 data.

compare with the 3A11 rain rates. During the TRMM boost period, F13 is in nominal operating conditions. Ten years of F13 SSM/I and TMI data (1998–2007) are included and examined in this study.

Fig. 2 shows the time series of rain rates from SSM/I, 3A11, and modified 3A11. Only collocated data among these data sets are used for comparisons. The ten-year mean rain rates are 3.06, 2.74, and 2.82 mm/day for SSM/I, 3A11, and modified 3A11, in that order. The SSM/I rain rates are higher than the 3A11 rain rates throughout the entire period; however, in this study, we focus only on the discontinuity of 3A11 time series due to the boost effect. To clearly see the boost effect on 3A11 rain rates, the time series of the differences between 3A11 and SSM/I rain rates with and without boost correction are shown in Fig. 3. Similar to the results of Shin and Chiu [2], the rain-rate differences between preboost and postboost without any correction are statistically significant. To calculate the mean difference, the August 2001 data are not included in the computation. The mean difference during the preboost period is calculated to be $-0.241$ mm/day. When the modified $T_b-R$ relation is applied in METH algorithm to the postboost data, the mean difference is improved to

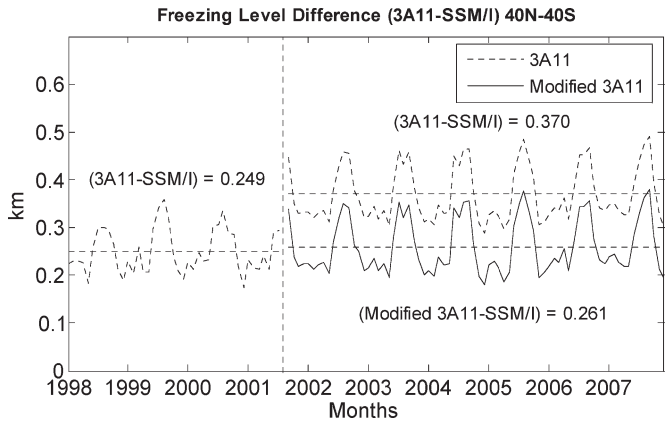


Fig. 4. Same as Fig. 3 except for freezing levels.

$-0.238$ mm/day when compared with the $-0.367$ mm/day of the one without modification. A student's $t$-test shows no significant difference between preboost and postboost periods after modification.

The freezing level, a proxy variable for determining the melting level and the atmospheric water-vapor content, is also examined. Fig. 4 shows the time series of the difference of freezing levels between SSM/I and 3A11 with and without modification of $T_b-R$ relation. Overall, the 3A11 freezing levels are higher than the SSM/I. The jump after August 2001 in freezing level due to the boost effect is also detected. The mean retrieved freezing level for the postboost period is about 0.12 km higher than the preboost period. After a modified $T_b-R$ relation is applied, the mean freezing level difference is reduced to 0.26 km, which is virtually identical to the difference during the preboost period (0.25 km).

Table I summarizes our results and compares the two approaches of $T_b$ adjustment and the use of postboost $T_b-R$ relation. From Shin and Chiu [2], the differences between the preboost and postboost periods are $-0.185$ mm/day for rain rate and 0.113 km for freezing level. $T_b$-adjustment reduces the differences to $-0.01$ mm/day and $-0.17$ km, or 5% and 15%, respectively, for rain rate and freezing level. If the proper physics is taken into account, using the same radiative transfer model for the postboost orbital parameters, the modified algorithm reduces the differences from $-0.126$ to 0.003 mm/day for rain rate and from 0.121 to 0.012 km for freezing level, which represents reductions to 3% and 10%, respectively. These differences, albeit small, have significant implications for intersatellite calibration and climate-change detection.

## IV. Climate Trends

To show the improvement of the modified 3A11 rain rates for climate studies, linear-trend analyses of these oceanic rainfall products are carried out for this time period. Fig. 5 shows the time series of domain (40 S–40 N) average of the 3A11, modified 3A11, and SSM/I oceanic nonseasonal rainfall. Nonseasonal rainfall is the departure of the monthly mean from the climatological average over all the years. The time series

TABLE I
SUMMARY OF RESULTS FOR PREBOOST AND POSTBOOST BIASES FOR THE UNCORRECTED, $T_b$-ADJUSTED (SHIN AND CHIU), AND MODIFIED ALGORITHM (THIS PAPER). RESULTS FOR THE MODIFIED ALGORITHM ARE COMPUTED FROM 1998 TO 2007. THE $T_b$-ADJUSTED ALGORITHM IS COMPUTED FROM 1998 TO 2005, AND THE NUMBERS ARE TAKEN FROM SHIN AND CHIU. THE NUMBERS SHOWN IN THE TABLE FOR THE MODIFIED ALGORITHM DO NOT INCLUDE AUGUST 2001. $*$ INDICATES SIGNIFICANT DIFFERENCE AT 95% USING A STUDENT'S $t$-TEST AGAINST THE NULL HYPOTHESIS OF NO DIFFERENCE BETWEEN THE PRE- AND POSTBOOST PERIODS

| 3A11 – SSM/I | Modified Algorithm | | | $T_b$-Adjusted | | |
|---|---|---|---|---|---|---|
| | preboost | postboost | difference | preboost | postboost | difference |
| Rain Rate (mm/day) | | | | | | |
| uncorrected | -0.241 | -0.367 | -0.126* | -0.223 | -0.408 | -0.185* |
| corrected | | -0.238 | 0.003 | | -0.233 | -0.010 |
| Freezing Level (km) | | | | | | |
| uncorrected | 0.249 | 0.370 | 0.121* | 0.258 | 0.371 | 0.113* |
| corrected | | 0.261 | 0.012 | | 0.241 | -0.017 |

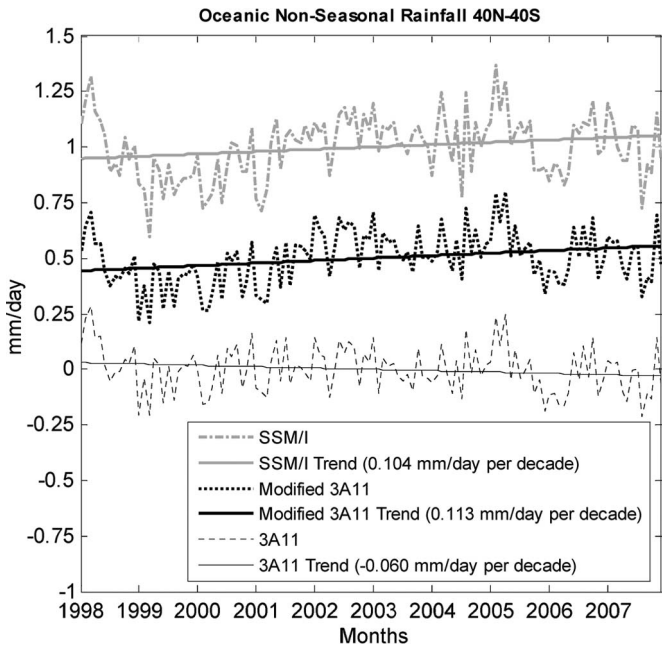


Fig. 5. Comparisons of linear-trend analyses of 3A11, modified 3A11, and SSM/I oceanic nonseasonal rainfall. The plots are shifted by 1 and 0.5 mm/day for SSM/I and modified 3A11, respectively.

of SSM/I and modified 3A11 nonseasonal rainfall track along with each other quite well. The correlation with SSM/I time series is improved from 0.78 to 0.90. The solid lines represent linear-trend analyses performed on these time series. Linear-trend herein is defined as the slope of the linear regression of the time series. Significance of the trends is tested using a two-tail student's $t$-test. Results show a decreasing trend ($-0.060$ mm/day per decade) for the unmodified 3A11 in contrast to an increasing trend of 0.113 mm/day per decade for the modified 3A11. The corresponding increase of the F13 SSM/I METH rain rates is 0.104 mm/day per decade.

The upper panel of Fig. 6 shows the spatial pattern of the trend from linear regression analyses for the modified 3A11 computed from ten-year nonseasonal rain rates. Increasing trends occur in the intertropical convergence zone (ITCZ) and the South Pacific convergence zone. However, regions of decrease are found in the east Pacific of the ITCZ, the east Indian Ocean between 5 N–25 N and the west Pacific to the east of Australia. The trend pattern for the unmodified algorithm (not shown) is totally different. The linear-trend pattern for the F13 SSM/I METH rain rates is shown on the lower panel of Fig. 6. The trend patterns between these two rain products are relatively similar and comparable to the trends found in Chiu and Chokngamwong [7].

## V. CONCLUSION

After being boosted into a higher orbit, the characteristics of the instruments onboard the TRMM satellite have been affected. Small changes in $T_b$ can contribute to significant changes in rain rates. For the postboost TMI, the microwave $T_b$ is increased due to the increase in the Earth incidence angle, the footprint diameter, and the swath width. Without $T_b$ adjustments, the difference of 3A11 and SSM/I shows a significant jump between preboost and postboost data [2]. They modified the algorithm by constantly subtracting the increased $T_b$ of 1.67 K from the postboost data to be consistent with the preboost data. In this paper, a $T_b-R$ relation is recomputed from the radiative transfer model of Wilheit *et al.* [3] for the postboost period. The 3A11 algorithm is modified to accept two $T_b-R$ relations for the preboost and postboost era, respectively, without any $T_b$ adjustment. As the TRMM data products are expected to be periodically reprocessed, the new version (version 7) of the 3A11 rain product will be reprocessed using the modified 3A11 algorithm.

Linear-trend analyses show that trends for modified 3A11 rain rates are significantly improved over the unmodified 3A11. An increasing trend is found to be consistent in magnitude and pattern with trends analyzed from GPCP and METH rain rates using the Remote Sensing System Version 6 SSM/I brightness temperature data. That two very different analyses of the microwave radiometer data yield similar results adds credibility to the increasing rainfall trend.

In summary, an effort has been made to investigate the effects of the TRMM orbit boost on the 3A11 algorithm, and we demonstrate the robustness of the METH algorithm. By modifying the appropriate orbital parameters of TMI, changes in the $T_b$ are effectively accounted for in the modified algorithm for postboost TMI data. Comparison with F13 SSM/I METH estimates shows that boost effect has been accounted for, without ad-hoc adjustments in the $T_b$. If we consider the preboost and

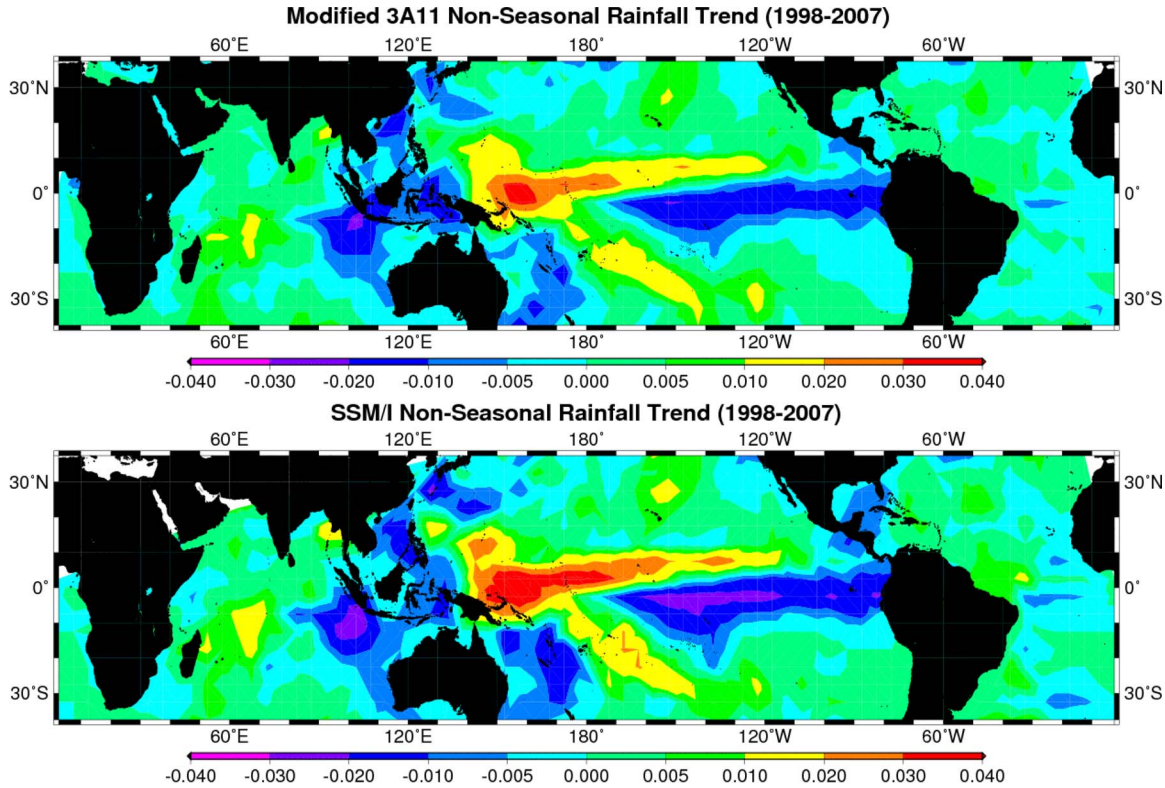


Fig. 6. Patterns of linear-trends of (upper panel) ten-year modified 3A11 nonseasonal rainfall and (lower panel) METH applied to F13 SSM/I. The trend is defined as a slope of the linear regression in units of millimeters per day per month.

postboost TMI as two different sensors, the METH technique effectively accommodates the sensor changes, and hence, its adaptability to different sensors for climate-scale analysis is demonstrated.

## ACKNOWLEDGMENT

The authors would like to thank Dr. R. Adler for helpful discussions. The TRMM algorithm trending data are available from the NASA/GSFC Precipitation Processing System URL: http://pps.gsfc.nasa.gov/tsdis/trending/rp_trending/trending.html. The F13 METH rain-rate data are available from the GPCP-Polar Satellite Precipitation Data Center (URL: http://gpcp-pspdc.gmu.edu/).

## REFERENCES

[1] T. T. Wilheit, A. T. C. Chang, and L. S. Chiu, "Retrieval of monthly rainfall indices from microwave radiometric measurements using probability distribution functions," *J. Atmos. Ocean. Technol.*, vol. 8, no. 1, pp. 118–136, Feb. 1991.

[2] D. B. Shin and L. S. Chiu, "Effects of TRMM boost on oceanic rainfall estimates based on Microwave Emission brightness Temperature Histograms (METH)," *J. Atmos. Ocean. Technol.*, vol. 25, no. 10, pp. 1888–1893, Oct. 2008.

[3] T. T. Wilheit, A. T. C. Chang, M. S. V. Rao, E. B. Rodgers, and J. S. Theon, "A satellite technique for quantitatively mapping rainfall rates over the oceans," *J. Appl. Meteorol.*, vol. 16, no. 5, pp. 551–560, May 1977.

[4] R. F. Adler, G. Gu, J. J. Wang, G. J. Huffman, S. Curtis, and D. Bolvin, "Relationships between global precipitation and surface temperature on interannual and longer timescales (1979–2006)," *J. Geophys. Res.*, vol. 113, no. D22, p. D22 104, Nov. 2008. DOI: 10.1029/2008JD010536.

[5] K. A. Hilburn and F. J. Wentz, "Intercalibrated passive microwave rain products from the unified microwave ocean retrieval algorithm (UMORA)," *J. Appl. Meteorol. Climatol.*, vol. 47, no. 3, pp. 778–794, Mar. 2008.

[6] G. J. Huffman, R. F. Adler, D. T. Bolvin, and G. Gu, "Improving the global precipitation record: GPCP Version 2.1," *Geophys. Res. Lett.*, vol. 36, no. 17, p. L17 808, Sep. 2009. DOI: 10.1029/2009GL040000.

[7] L. S. Chiu and R. Chokngamwong, "Microwave Emission brightness Temperature Histograms (METH) rain rates for climate studies: SSM/I V6 results," *J. Appl. Meteorol. Climatol.*, vol. 49, no. 1, pp. 115–123, Jan. 2010.

[8] L. S. Chiu, R. Chokngamwong, Y. Xing, R. Yang, and C.-L. Shie, "Trends and variations of global oceanic evaporation datasets from remote sensing," *Acta Oceanologica Sin.*, vol. 27, no. 3, pp. 1–12, 2008.

[9] T. Kubota, S. Shige, H. Hashizume, K. Aonashi, N. Takahashi, S. Seto, M. Hirose, Y. N. Takayabu, K. Nakagawa, K. Iwanami, T. Ushio, M. Kachi, and K. Okamoto, "Global precipitation map using satellite-borne microwave radiometers by the GSMaP project : Production and validation," *IEEE Trans. Geosci. Remote Sens.*, vol. 45, no. 7, pp. 2259–2275, Jul. 2007.

[10] T. Tagawa, H. Hanado, S. Shimizu, and R. Oki, "Improved correction of beam mismatch of the precipitation radar after orbit boost of the TRMM satellite," *IEEE Trans. Geosci. Remote Sens.*, vol. 47, no. 10, pp. 3469–3479, Oct. 2009.

[11] J. S. Marshall and W. M. Palmer, "The distribution of rain drops with size," *J. Atmos. Sci.*, vol. 5, no. 4, pp. 165–166, Aug. 1948.

[12] S. A. Wang, "Modeling the beamfilling correction for microwave retrieval of oceanic rainfall," Ph.D. dissertation, Dept. Meteorol., Texas A&M Univ., College Station, TX, 1995.

[13] L. S. Chiu, G. R. North, D. A. Short, and A. McConnell, "Rain estimation from satellites: Effect of finite field of view," *J. Geophys. Res.*, vol. 95, no. D3, pp. 2177–2185, 1990.

[14] R. F. Adler, G. J. Huffman, A. Chang, R. Ferraro, P. Xie, J. Janowiak, B. Rudolf, U. Schneider, S. Curtis, D. Bolvin, A. Gruber, J. Susskind, and P. Arkin, "The version 2 Global Precipitation Climatology Project (GPCP) monthly precipitation analysis (1979–Present)," *J. Hydrometeor.*, vol. 4, no. 6, pp. 1147–1167, Dec. 2003.

**Long S. Chiu** (SM'06) was born in Hong Kong, in 1953. He received the B.S. degree in physics from the University of Miami, Coral Gables, FL, in 1974, and the Sc.D. degree in meteorology from the Massachusetts Institute of Technology, Cambridge, in 1980.

He was a Senior Scientist and Group Manager (1989–1998) with SAIC/General Sciences Corporation, Laurel, MD, a Contract Scientist with the NASA Goddard Space Flight Center, Greenbelt, MD, and a Visiting Scholar at the Center for Space and Remote Sensing Research, National Central University, Chung-Li, Taiwan (1992). He was a Research Professor (1998–2000) and has been a tenured Associate Professor (2001–present) with George Mason University, Fairfax, VA. He is currently a Professor with the Institute of Space and Earth Information Science, Chinese University of Hong Kong, Shatin, Hong Kong. His current research interests include microwave remote sensing, rainfall estimation and analysis, climate change and variability, and aerosol–cloud–precipitation interactions.

Prof. Chiu is a Fellow of the Electromagnetics Academy, a member of the American Meteorological Society, American Geophysical Union, Sigma Xi, Sigma Pi Sigma, Past President (2004–2006) of the Chinese–American Ocean-Atmosphere Association, and President (2007–2009) of the Hong Kong Society of Photogrammetry and Remote Sensing.

**Roongroj Chokngamwong** received the B.S. degree in electrical engineering from Thammasat University, Bangkok, Thailand, in 1998, the M.S. degree in computer science from The George Washington University, Washington, DC, in 2001, and the Ph.D. degree in computational sciences and informatics from George Mason University (GMU), Fairfax, VA, in 2007.

In 2001, he was a Software Developer and a System Administrator with Supply Chain Intelligence, Inc., Cary, NC. In 2002, he was with the Center for Earth Observing and Space Research (CEOSR), GMU, as an Assistant System Administrator and a Research Assistant while working toward the Ph.D. degree. He was also a Research Associate with CEOSR in 2007. Since March 2008, he has been a Postdoctoral Fellow with the Institute of Space and Earth Information Science, Chinese University of Hong Kong, Shatin. His current research interests include satellite rainfall-estimation algorithms, Earth-observing and remote-sensing applications, and statistics modeling and data analyses.

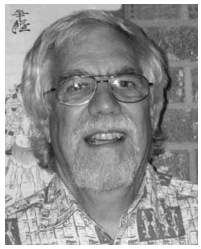

**Thomas T. Wilheit** (M'75–SM'76–F'04–LF'09) received the Ph.D. degree in physics from the Massachusetts Institute of Technology, Cambridge, in 1970.

From 1970 to 1989, he was with the NASA Goddard Space Flight Center, Greenbelt, MD, where he was the Head of the Microwave Sensors Branch, one of the various positions he held. He is currently a Professor with the Department of Atmospheric Science, Texas A&M University, College Station, where he has taught since 1989. He has written several papers on various aspects of passive microwave remote sensing.

Dr. Wilheit is a member of the American Geophysical Union, American Association for the Advancement of Science, International Scientific Radio Union (URSI) Commission F, and Committee for Space Research (COSPAR) Commission A. He is a Fellow of the American Meteorological Society.